IUTAM Symposium on Dynamics of Capsules, Vesicles and Cells in Flow

Hydrodynamic focusing of an elastic capsule in Stokes flow: An exploratory numerical study

Cecilia Rorai[a,b,*], Francesca Nason[c], Lailai Zhu[a], Giustina Casagrande[c], Gabriele Dubini[c], Luca Brandt[a]

[a]Linné Flow Centre, KTH Mekanik, Osquars Backe 18, SE-10044 Stockholm, Sweden;
[b]Nordita, Roslagstullsbacken 23, 106 91 Stockholm, Sweden;
[c]Chemistry, Materials and Chemical Engineering Department "Giulio Natta", Politecnico di Milano, Milano, Italy

Abstract

We study numerically the motion of an elastic capsule in a simple microfluidic device, a sheath flow focuser, designed to align (or focus) particles at the center of a microchannel. The geometry of the device is given, while the flow conditions are varied, and the outflux is constant. The efficiency is expressed in terms of the distance required to achieve focusing and the functioning is characterized by the deformations and stresses undergone by the capsule membrane. Calculations are performed for a 'stiff' and 'soft' capsule, corresponding to a capillary number equal to $Ca = 0.05$ and $Ca = 0.3$ based on the outflow rate. We report that as the sheath flow is increased the focusing efficiency grows and plateaus beyond a certain threshold, displaying a drop in the efficiency gain. Differently, the deformations and stresses undergone by the capsule membrane grow for the entire range of the flow parameters considered. This should be kept in mind if the stresses exerted on the membrane have to be minimized or need to be below certain characteristic thresholds typical of the specific application considered. Especially large initial offsets and stiff capsules benefit from focusing.

Keywords: hydrodynamical focusing; elastic capsules; microfluidic devices

1. Introduction

Diseases are known to alter the complex biochemical mechanisms that regulate the life of cells by also affecting their mechanical characteristics. Mechanical anomalies can be identified by using specific microfluidic devices designed in such a way that cells with different size, shape, or deformability, follow distinct and separate trajectories and are collected downstream in different positions.[1,2,3] This is a recent and active field of research in medical diagnostics that draws attention to mechanical properties as relevant markers for cells. In contrast to biochemical markers, employed in traditional medical diagnostics, biophysical markers are label free, low cost, and characterized by shorter

---

* Corresponding author. Tel.: +46 769 253 364; fax: +46 855 378 404.
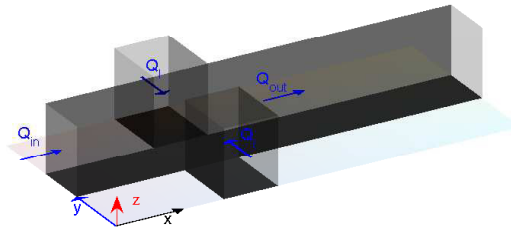 *E-mail address:* crorai@kth.se

Fig. 1. Three-dimensional sketch of the computational domain. The fluid flows in the direction of the blue arrows: along the *x*-axis in the main duct, along positive/negative *y* to converge into the main duct in the lateral 'branches'. The flux entering the main duct is Q_{in}, the flux coming from each lateral duct is Q_l, their sum gives an outflux, Q_{out}, which is kept constant in our calculations. The duct cross-sections measure $5a_c$ (depth) along *z* and $4a_c$ (width) along *y* (along *x* in the lateral arms of the cross). The main channel is $30a_c$ long and intersects the lateral ducts between $-2 < x < 2$. Equal fluxes come from the lateral 'branches, but the $\kappa = 2Q_l/Q_{in}$ ratio can be tuned to control the focusing efficiency.

assay times and larger throughput. Hence, they offer remarkable advantages with a view to quick preliminary diagnoses.

For sorting devices to give reliable outputs, cells often need to be aligned at the inlet, as is the case of the sorting device proposed in Ref. 3. This is a delicate task which is achieved by focusing devices.[4] In this article we study the functioning and efficiency of a simple microfluidic device, a sheath flow focuser (see Figure 1), that allows for an effective alignment (or focusing) of cells with different deformabilities or flowing at different flow rates. Focusing particles into a tight stream is usually also a necessary step prior to counting and detecting them in microfluidic sensing devices,[5] and prevents them from being adsorbed to channel walls.[4] It may be counter-argued that from a theoretical point of view there is little need for focusing to individually interrogate particles since it is possible to manufacture sufficiently narrow channels to force the particles into a single file. However, the use of narrow channels raises the risk of clogging and surface fouling. Significant back pressure and shear stresses may also occur when driving fluid through such small channels, which increases instrument costs and can damage the cells under investigation.[6]

A device similar to the one shown in Figure 1, has been used for the characterization of red blood cell deformability change during blood storage,[7] and may be exploited for entrapment of chemicals, drug, proteins, etc. in erythrocytes by virtue of the stresses it exerts on the cell membrane. In fact, the majority of the methods for the entrapment in erythrocytes takes advantage of the remarkable capacity of this cell for reversible shape changes and for reversible deformation under stress,[8,9] allowing transient opening of pores large enough to be crossed by externally placed macromolecules. The main are: i) Electroporation; ii) Drug-induced endocytosis; iii) Osmotic pulse method; iv) Hypotonic hemolysis.[10] In our calculations the stress and deformability can be estimated with the hope of identifying a range of flow parameters where entrapment can be achieved experimentally.

After describing the mathematical and numerical methods used to approach this problem, we present our set up (the numerical domain and the boundary and initial conditions) and define the flow parameters. The results in the focusing device are introduced by first commenting on the flow of a capsule in a straight channel. A series of calculations are performed in this simpler set up and will serve as reference cases to be compared to simulations in the focusing device. We characterize the functioning of the focusing device when varying the flow parameters for a range of initial positions of the capsule. We plot the trajectories and shapes of the capsules along their path and estimate the downstream distance where the capsule centroid is 0.2 radii apart from the channel midline. We look at the behavior of quantities such as the maximum stress and the fractional change in surface area.

2. Methods

2.1. Mathematical model

As a first remark, note that typical cell sizes measure few tens of micrometers. Microfluidic devices designed to manipulate them have widths of the same order of magnitude, and characteristic velocities between a few *μm/s* to a

few cm/s for single file cell devices.[2,11,4] Given the small sizes and velocities involved, it is justified to model the fluid flow by neglecting the inertial effects and by reducing the Navier-Stokes equations to the linear Stokes equations.

In our study, capsules are regarded as fluid-filled closed membranes of elastic material, two-dimensional and isotropic. Their deformations are measured as the displacements from a reference shape that is assumed to be spherical with radius a_c. We have chosen to describe the capsule through a neo-Hookean constitutive law according to which the local strain energy function is

$$W = \frac{G_s}{2}\left[\mathcal{I}_1 - 1 + \frac{1}{\mathcal{I}_2 + 1}\right],$$ (1)

where G_s is the isotropic shear modulus, while $\mathcal{I}_1 = \lambda_1^2 + \lambda_2^2 - 2$ and $\mathcal{I}_2 = \lambda_1^2\lambda_2^2 - 1$ are the two invariants of the left Cauchy-Green tensor expressed in terms of the eigenvalues, λ_1, λ_2, of the two-dimensional strain matrix, also referred to as the principal stretch ratios.

We employ a linear isotropic model for the bending moment,[12] with a bending modulus $G_b = C_b a_c^2 G_s$, where $C_b = 0.01$ is held constant in our simulations; this value is consistent with available experimental data for RBCs.[13] We consider the bending modulus of RBCs since our numerical work is motivated by (but not limited to) applications that mainly involve erythrocytes as discussed in the introduction. This choice is supported by the fact that neo-Hookean capsules are accepted as a reasonable model to describe the hydrodynamical behavior of RBCs[13]. Values of the bending modulus for other types of cells or manufactured capsules are not easily found. Whether the stress-free shape of RBCs should be assumed to be spherical or biconcave is still the subject of debate.[14] Some numerical studies performed in low shear-rate flow suggest, by comparison with experimental measurements, that the stress-free state of RBCs is a spheroid close to a sphere.[15] Finally we also assume that the fluid inside and outside the cell has exactly the same density and viscosity.

The surface of the capsule is discretized by N points and moves with the flow obeying no-slip, non-penetrating boundary conditions. The velocity field displaces the surface of the capsule out of its equilibrium configuration causing a back-reaction of the membrane to the flow that enters the flow equation as a forcing term $\mathbf{F} = \sum_{j=1}^{N} f_j\delta\left(x - x_j\right)$. Hence, the overall flow field results from the superposition of responses induced by each single point force (Green functions) acting on the surface of the capsule and on the walls.

The full set of equations includes the three-dimensional Stokes equation, the continuity equation for an incompressible flow and the equation to evolve the surface of the capsule

$$-\nabla p + \mu\nabla^2\mathbf{u} = -\sum_{j=1}^{N} f_j\delta\left(x - x_j\right),$$ (2)

$$\nabla \cdot \mathbf{u} = 0,$$ (3)

$$\frac{dx_j}{dt} = \mathbf{u}(x_j).$$ (4)

Here p is the pressure, $\mathbf{u}$ is the velocity, and μ is the dynamic viscosity of the fluid.

2.2. Numerical methods

Equations (2)-(4) are solved by a hybrid Integral-Mesh method,[16,17,13] more precisely, a boundary integral algorithm accelerated by the General Geometry Ewald like method (GGEM).[17,16] The GGEM method decomposes the force per unit volume exerted by the deforming surface on to the fluid into a local part and a global part and has already been used in a variety of micro-multiphase simulations.[18,19,20] The local problem accounts for the singular and short-ranged interaction while the global problem for the smooth and long-ranged interactions. In our implementation the global solution is computed with the Stokes module of the open-source Navier-Stokes solver NEK5000[21] using the spectral element method. As akin to FEM, the physical domain is decomposed into elements subdivided into arrays of Gauss-Lobatto-Legendre (GLL) nodes for the velocity and Gauss-Legendre (GL) nodes for the pressure field. This is the mesh-based part of the code which allows us to cope with non-trivial boundaries. The short-range part is handled instead by boundary integral techniques with singular and nearly-singular integration. The velocities of the Lagrangian points x_j on the capsule membrane are obtained by summing up the local and global velocities. We

use a third-order Adam-Bashforth time-integration scheme to update the position of those points. We use a spectral discretization [12] to calculate f_j given the positions x_j, i.e. to solve the membrane stress balance. A more detailed description of the numerical algorithm and its validation can be found in Ref. 22,23,24.

2.3. Relevant parameters and computational domain

If U is the bulk flow velocity, the dimensionless number that characterizes this problem is the capillary number, $Ca \equiv \mu U / G_s$, that expresses the ratio between the viscous forces and the elastic forces. Given the same flow conditions, larger capillary numbers refer to softer capsules.

Calculations are performed in a sheath flow focuser, whose shape and dimensions are sketched in Figure 1. The outflux, Q_{out}, is the same in all the simulations, while the influx from the main duct, Q_{in}, and the two lateral arms, Q_l, is varied according to the parameter κ:

$$\kappa = \frac{2Q_l}{Q_{in}}, \quad \text{with} \quad Q_{out} = Q_{in} + 2Q_l.$$

Note that the average flow velocity U that enters the definition of the capillary number is measured downstream with respect to the focusing and is associated to the outgoing flow Q_{out}. We perform calculations for two capillary numbers: $Ca = 0.05, 0.3$, eight flow regimes $0 < \kappa < 4$, and various y-offsets from the main duct mid-line ($y = 0, z = 0$). A y offset is a displacement in height (h) with respect to the mid line. The initial displacement is named h_{ini} and the evaluated conditions are $h_{ini} = 0.1, 0.5, 0.75, 0.85$. Capsules are released with a stress free spherical shape.

The channel cross-sections are rectangular of size $4a_c \times 5a_c$, as described in the caption of Figure 1, a velocity flow profile is imposed at the inlet according to equation (7) of Ref. 25, no slip and no penetrating boundary conditions are imposed on the solid walls and zero-stress boundary conditions, $-p\mathbf{I} + \mu \left(\nabla \mathbf{u} + (\nabla \mathbf{u})^T \right) = 0$, are imposed at the outlet.

3. Results

3.1. Simple focusing in a straight channel

It has been shown that elastic capsules in straight tubes and channels migrate toward the midline $y = 0, z = 0$, with a characteristic speed that depends on the capillary number. [26,27] Stiff capsules have longer migration times than soft ones. Hence, the simplest device to focus capsules is a long straight duct. Given our numerical setup, it is expensive to perform calculations in a straight channel long enough to observe capsules with the largest initial offsets approach the centerline to a distance of $0.2a_c$ or less. This requires, in fact, long domains and large meshes and has been circumvented by adopting a different strategy that consists of two steps. First, we perform long runs in a straight channel holding the centroid of the capsule fixed at a certain x-position, specifically $x = 0$. This is done by subtracting from each point on the surface of the capsule, at each time step, the distance that the capsule centroid has advanced in x during the previous time step. The distance covered (and subtracted at each step) is saved as output data, so that the trajectory in the $x - y$ plane can be plotted. Various runs for different initial offsets have been performed in this way. The resulting trajectories have been collapsed by shifting them along x and averaged to give a *reference curve* for the approach to the channel centreline. The optimal shift is the one that minimizes the area between the two curves and is found recursively with a bisection algorithm. These reference curves for $Ca = 0.05, 0.3$ are shown in black in Figure 2, together with the curves they have been obtained from (shown in color) shifted to give the optimal overlap. The reference curves give indication of the expected trajectory for a capsule of given capillary number placed at initial offset $h_{ini} = 0.85$ or less. Observe the faster decay for $Ca = 0.3$ for which it has been possible to follow the capsule to a distance $y < 0.05a_c$ from the midline. Curves obtained from runs with different initial offsets match better when collapsed for softer capsules. This suggests that the trajectory of stiff capsules is more affected by the initial condition and it is therefore less accurate to predict it from some average behavior. From these results it is confirmed that soft capsules approach the mid-plane more rapidly. The migration velocity slows down as the mid-line of the channel is approached.

Since the capsule is off-center it experiences a non symmetric flow velocity with respect to its centroid. This causes a non-symmetric deformation with respect to the centroid as seen in Figure 3 and a tank-treading motion of
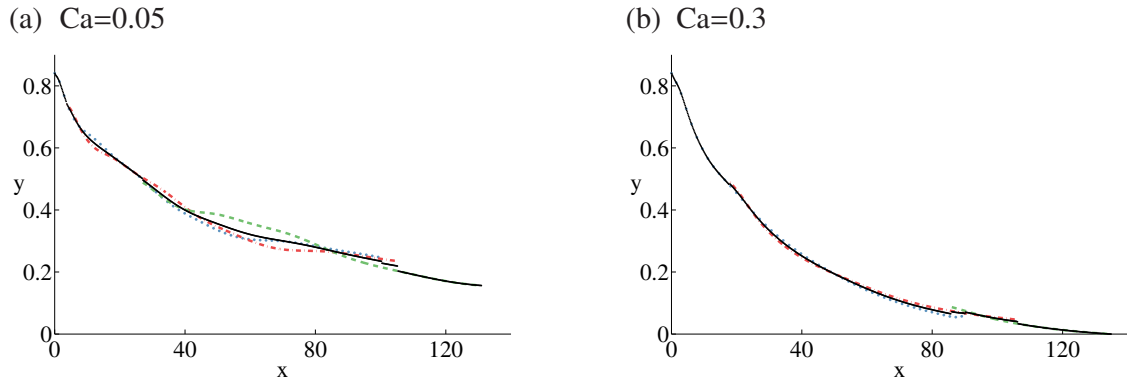
Fig. 2. Position of the capsule centroid along the *y* axis versus its streamwise position *x* for *Ca* = 0.05 (a), and *Ca* = 0.3 (b). The black curves are reference curves computed by averaging the colored curves obtained from three separate runs: h_{ini} = 0.5, 0.75, 0.85 in (a), h_{ini} = 0.1, 0.5, 0.85 in (b). The curves are collapsed as described in the text. Observe the faster decay and the better collapse for *Ca* = 0.3, which suggests that the trajectory of stiff capsules is more affected by the initial condition.
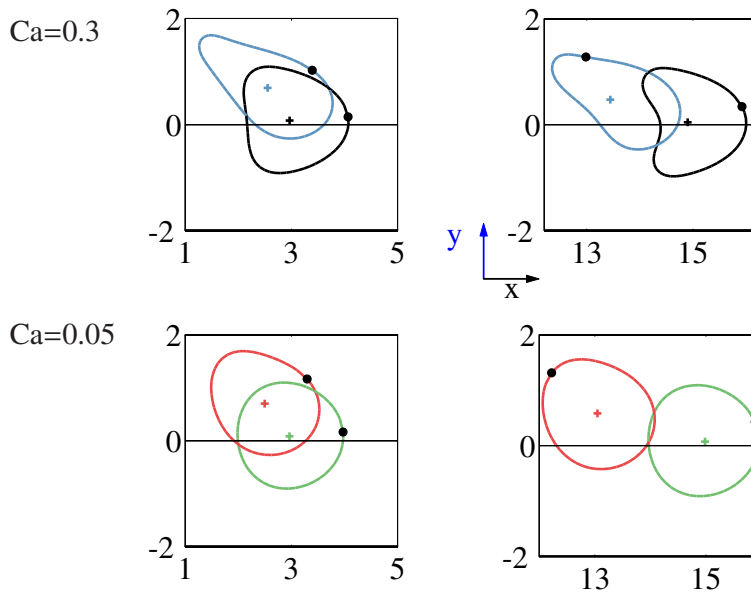

Fig. 3. Shapes on the *z* = 0 plane of stiff (top) and soft (bottom) capsules soon after they are released (left) and about $15a_c$ units downstream (right). Capsules are released at *x* = 0 with a stress free spherical shape. We show the results for the runs with h_{ini} = 0.1 (black and green) and h_{ini} = 0.75 (blue and red). The cross marks the capsule centroid, the black dot marks the position of a material point that changes its relative position on the membrane as a consequence of the tank treading motion.

the membrane, as highlighted by the black marker in the plot. Note that the results for a straight duct will certainly also depend on the ratio between the width and depth of the duct and the capsule radius a_c. These dependences are not analyzed in the present study. The reference curves will be used to estimate the trajectories in the straight channel past the focusing device in the next section.
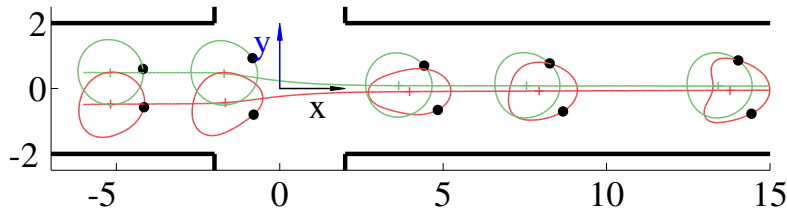
Fig. 4. Stiff (green) and soft (red) capsule shapes along the trajectory in the focusing device for $\kappa = 3$. We calculate a single capsule trajectory at the time, we plot two for comparison. The shapes are shown at the same time. Focusing is specially effective on stiff capsules, otherwise characterized by lower migration velocities.
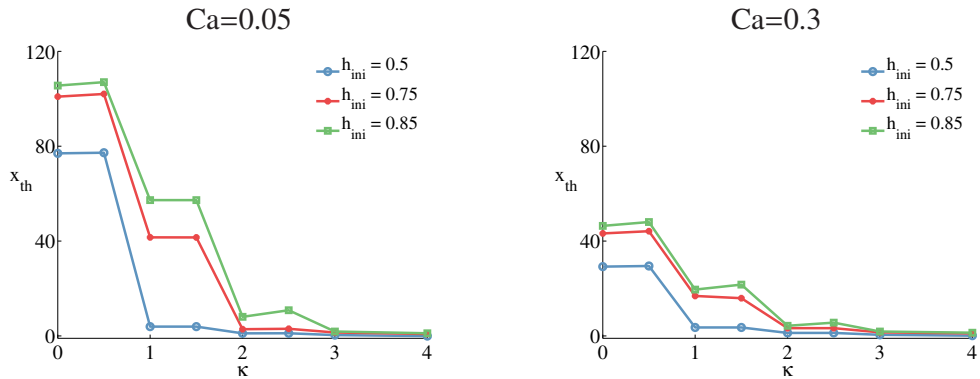

Fig. 5. Distance from the center of the focusing device, $x = 0$, where we expect the centroid of the capsule to have approached the duct midline by a distance equal to 20% of its radius. The results are plotted for different initial offsets as reported in the legend. For many of our runs this distance is not reached by the end of the calculations and it has been necessary to fit the last part of the trajectory with a reference curve following a procedure described in the text.
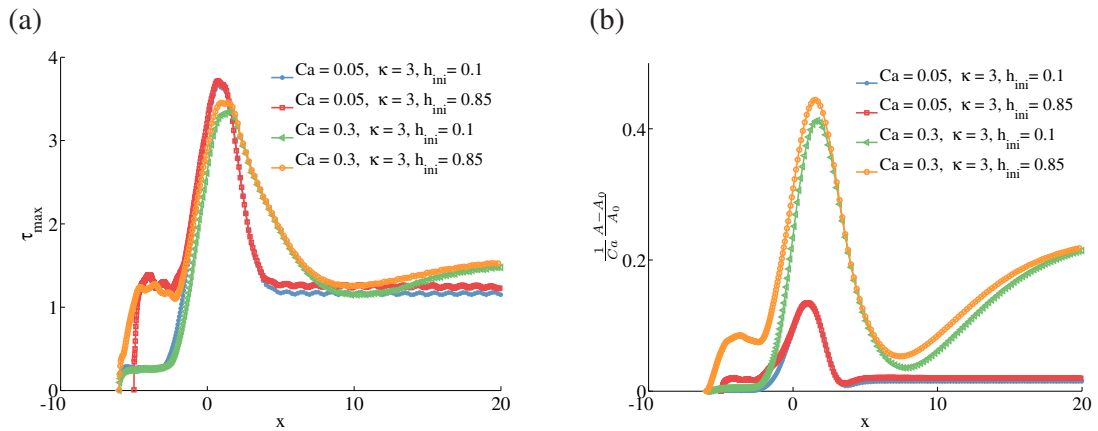

Fig. 6. (a) Maximum local stress as a function of the x-position of the center of mass. (b) Fractional change in area as a function of the x-coordinate of the center of mass scaled by the capillary number. Data are reported for the runs listed in the legend. We compare the behavior of the stiff and soft capsule for the largest and smallest offsets considered, intermediate offsets display intermediated behaviors.
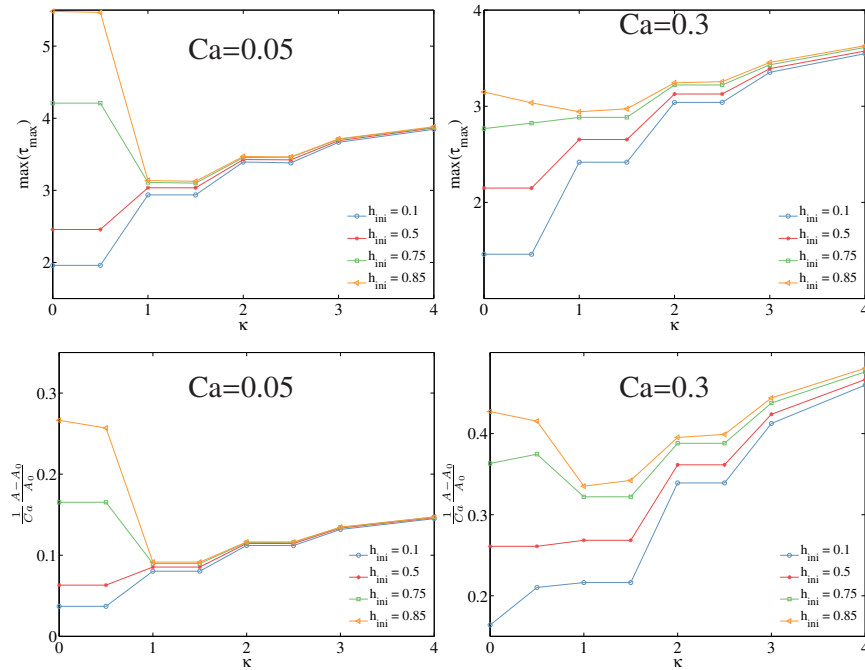
Fig. 7. Maximum local stress (top), and maximum fractional change in area (bottom) as a function of κ for the offsets reported in the legend.

3.2. Motion in the focusing device

The behavior in the proposed focusing device depends on several parameters, some associated with the geometry of the device (width, depth and length of the channel), some with the initial condition (the initial offset, h_{ini}, and shape of the capsule), and some with the flux and elastic properties of the material, embodied in the capillary number Ca and κ. The purpose of this exploratory study is to investigate, specifically, the role of three of them: the capillary number Ca, the initial offset h_{ini}, and the flux conditions controlled by tuning the parameter κ. Note that the case $\kappa = 0$ corresponds to no-flow coming from the lateral channels, and as such is expected to yield different results from the case of a straight channel. In fact, the focusing region becomes an expansion region for the flow.

In Figure 4 we show the shape of a stiff and soft capsule along its trajectory in the focusing device. As expected, the softer capsule (red) deforms more and approaches the channel midline more rapidly. The outlet is located 20 units downstream with respect to the focuser, while the calculations are stopped when the centroid reaches $x = 15$, before the outflow boundary condition may affect the result. Depending on the capillary number, κ, and h_{ini}, the capsule centroids exit the device at a different $y-$position. However, ideally, we would like to know how long the channel needs to be for the centroid to reach a certain offset from the midline, namely a threshold y_{th}, below which we consider the capsule to be reasonably centered. We have chosen the value $y_{th} = 0.2a_c$ and denote the distance from the focusing where this threshold is reached as x_{th}.

The value of x_{th} is estimated by comparing the trajectories of the capsules exiting the focusing device for $x > 5$, with the reference curves for an infinitely long straight channel shown in Figure 2. The fitting is performed by following the procedure described in the previous section: the reference curve is shifted along x through a recursive bisection algorithm until the area between the trajectory of the capsule past the focusing and the reference curve is minimized. There is an almost perfect overlap when considering the $Ca = 0.3$ case, while the accuracy of the result is lower for $Ca = 0.05$. The results are reported in Figure 5 for the two capillary numbers under consideration. The quantity x_{th} is plotted as a function of κ for different initial offsets. Larger κs guarantee a better focusing, as expected; however, x_{th} seems to plateau as κ increases suggesting a drop in the efficiency gain. Especially large initial offsets and stiff capsules benefit from focusing. The data seem to indicate that soft capsules are more efficiently centered

than stiff ones for low κ (compare the left and right panel), which is consistent with the behavior in a straight channel: the migration velocity of soft capsules is larger than that of stiff ones. However, this is not the case for high κ, where focusing works equally well for $Ca = 0.05$ and 0.3. The threshold for which this is true depends on h_{ini}.

In Figure 6 we show the behavior of the maximum local stress τ_{max} and fractional change in area rescaled by Ca for the $h_{ini} = 0.1$ and 0.85 runs performed at $\kappa = 3$. The maximum is reached for $0 < x < 2$, around the center of the focusing area. The value of the maximum stress is comparable for the soft and sitff capsule, being slightly larger for the stiff one, while the fractional change in area is about three times larger for the largest Ca. Observe that interestingly both quantities grow downstream for the soft capsule. This is possibly explained by the fact that the capsule changes its shape from being elongated in x, in the focuser, to being stretched in y downstream. The transition implies going through an almost stress-free spherical shape. Differently, stiff capsules do not undergo dramatic shape changes but display a characteristic oscillatory behavior of the maximum local stress τ_{max}.

The maximum local stress and the maximum fractional change in area measured along the capsule trajectory are displayed in Figure 7 for all the runs performed in the focusing device. Both quantities grow with κ, except for $\kappa < 1$ and Ca=0.05 and $\kappa < 1$, Ca=0.3 and the largest offsets. In these cases the maximum is also registered at a different location along the trajectory: at the entrance of the focusing area ($x \approx -2$) rather than about its center, in contrast to what is reported in Figure 6.

4. Conclusions

We study numerically the motion of an elastic capsule in a sheath flow focuser, which is designed to align particles on a microchannel midline. The device consists of four microchannels merging at 90 degrees, as shown in Figure 1. The flow direction is indicated by blue arrows. The ratio between the flux coming from the lateral "arms" and the incoming flux in the main channel (oriented along x), is expressed by the parameter κ. The outflux is constant. Calculations are performed for a 'stiff' and 'soft' capsule, corresponding to a capillary number equal to $Ca = 0.05$ and $Ca = 0.3$ based on the outflow rate. The efficiency is expressed in terms of the distance required to achieve focusing. We observe that the effectiveness of focusing grows with κ and with the capillary number, until it plateaus. Differently, the deformations and stresses undergone by the capsule membrane seem to grow linearly for the entire range of the flow parameter. This should be kept in mind if the stresses exerted on the membrane have to be minimized or need to be below certain characteristic thresholds typical of the specific application considered. If so, the optimal parameter κ is likely an intermediate one. Observe also that, counterintuitively, small lateral fluxes, $\kappa < 1$, develop particularly large deformations and stresses for stiff capsules and large offsets. This is due to the fact that the focusing region becomes an area of expansion for the flow, causing the capsule to be pushed toward the corners of the focusing geometry. Two more interesting phenomena are the oscillations developed by the maximum stress for a stiff capsule [Figure 6(a)] and the downstream growth of stresses and deformations for the soft capsule [Figure 6(a)-(b)].

References

1. Mao, X., Huang, T.. Exploiting mechanical biomarkers in microfluidics. *Lab Chip* 2012;**12**:4006–4009.
2. Beech, J.P., Holm, S.H., Adolfsson, K., Tegenfeldt, J.O.. Sorting cells by size, shape and deformability. *Lab Chip* 2012;**12**(6):1048–1051.
3. Zhu, L., Rorai, C., Mitra, D., Brandt, L.. A microfluidic device to sort capsules by deformability: A numerical study. *Soft Matter* 2014; **10**:7705–7711.
4. Xuan, X., Zhu, J., Church, C.. Particle focusing in microfluidic devices. *Microfluid Nanofluid* 2010;**9**:1.
5. Kim, Y., Yoo, J.. Three-dimensional focusing of red blood cells in microchannel flows for bio-sensing applications. *Biosensors and Bioelectronics* 2009;**24**(12):3677–3682.
6. Ateya, D.A., Erickson, J.S., Jr, P.B.H., Hilliard, L.R., Golden, J.P., Ligler, F.S.. The good, the bad, and the tiny: a review of microflow cytometry. *Anal Bioanal Chem* 2008;**391**:1485–1498.
7. Zheng, Y., Chen, J., Cui, T., Shehata, N., Wang, C., Sun, Y.. Characterization of red blood cell deformability change during blood storage. *Lab Chip* 2014;**14**:577.

8. Guido, S., Tomaiuolo, G.. Microconfined flow behavior of red blood cells in vitro. *C R Physique* 2009;**10**:751–763.
9. Tomaiuolo, G., Guido, S.. Start-up shape dynamics of red blood cells in microcapillary flow. *Microvasc Res* 2011;**82**:35–41.
10. Magnani, M.. *Erythrocyte Engineering for Drug Delivery and Targeting*. Biotechnology intelligence unit 6. Landes Bioscience; 2002.
11. Kim, Y.W., Yoo, J.Y.. Axisymmetric flow focusing of particles in a single microchannel. *Lab Chip* 2009;**9**:1043.
12. Zhao, H., Isfahani, A.H.G., Olson, L.N., Freund, J.B.. A spectral boundary integral method for flowing blood cells. *J Comput Phys* 2010;**229**:3726–3744.
13. Freund, J.. Numerical simulation of flowing blood cells. *Annu Rev Fluid Mech* 2014;**46**(1):67–95. doi:10.1146/annurev-fluid-010313-141349.
14. Cordasco, D., Yazdani, A., Bagchi, P.. Comparison of erythrocyte dynamics in shear flow under different stress-free configurations. *Phys Fluids* 2014;**26**:041902.
15. Peng, Z., Mashayekh, A., Zhu, Q.. Erythrocyte responses in low-shear-rate flows: effects of non-biconcave stress-free state in the cytoskeleton. *J Fluid Mech* 2014;**742**:96.
16. Kumar, A., Graham, M.. Accelerated boundary integral method for multiphase flow in non-periodic geometries. *J Comput Phys* 2012;**231**:6682–6713.
17. Hernández-Ortiz, J., de Pablo, J., Graham, M.. Fast computation of many-particle hydrodynamic and electrostatic interactions in a confined geometry. *Phys Rev Lett* 2007;**98**(14):140602.
18. Kumar, A., Graham, M.. Segregation by membrane rigidity in flowing binary suspensions of elastic capsules. *Phys Rev E* 2011;**84**:066316.
19. Pranay, P., Anekal, S.G., Hernandez-Ortiz, J.P., Graham, M.D.. Pair collisions of fluid-filled elastic capsules in shear flow: Effects of membrane properties and polymer additives. *Phys Fluids* 2010;**22**:123103.
20. Pranay, P., Henríquez-Rivera, R.G., Graham, M.D.. Depletion layer formation in suspensions of elastic capsules in newtonian and viscoelastic fluids. *Phys Fluids* 2012;**24**:061902.
21. Fischer, P., Lottes, J., Kerkemeier, S.. nek5000 Web page. 2008. Http://nek5000.mcs.anl.gov.
22. Nason, F., Zhu, L., Dubini, G., Brandt, L.. Numerical simulation of a deformable cell in microchannels. In: S. Idelsohn, M.P., Schrefler, B., editors. *V International Conference on Computational Methods for Coupled Problems in Science and Engineering*. 2013, p. 1–11.
23. Zhu, L.. *Simulation of individual cells in flow. PhD thesis*. Royal Institute of Technology, KTH; 2014.
24. Zhu, L., Brandt, L.. The motion of a deforming capsule through a corner. *J Fluid Mech* 2014;**arXiv 1409.0155**:physics.flu–dyn.
25. Spiga, M., Morino, G.. A symmetric solution for velocity profile in laminar flow through rectangular ducts. *Int Commun Heat Mass Transfer* 1994;**21**(4):469–475.
26. Pozrikidis, C.. Numerical simulation of cell motion in tube flow. *Ann Biomed Eng* 2005;**33**:165–178.
27. Doddi, S.K., Bagchi, P.. Lateral migration of a capsule in a plane poiseuille flow in a channel. *Int j multiphase flow* 2008;**34**:966–986.